

Formation and Steady State Maintenance of FRCs Using Rotating Magnetic Field Current Drive

A.L. Hoffman, R.D. Brooks, J.A. Grossnickle, H.Y. Guo, K.E. Miller, R.D. Milroy,
A.M. Peter, Z.A. Pietrzyk, G.R. Votroubek

Redmond Plasma Physics Laboratory, University of Washington, Seattle, WA, USA

e-mail contact of main author: hoffman@aa.washington.edu

Abstract. Rotating Magnetic Fields (RMF) have been used to both form and sustain FRCs in cylindrical flux conservers. Penetration of the RMF into a conducting plasma cylinder is made possible by accelerating the electrons to rotate near synchronously with the RMF. When there are more than sufficient electrons, if rotating synchronously, to reverse the external confinement field, and when the force exerted by the RMF exceeds the electron-ion frictional force (resistivity), the electron slip will automatically adjust to provide just the degree of RMF penetration and current drive needed to maintain the FRC reversal current. The FRC flux will increase and the FRC will expand radially (and contract axially), increasing the plasma density until the RMF and resistive frictional forces are balanced. The plasma temperature will be determined by heating and loss rates, with the RMF penetration increasing automatically as the temperature rises to accommodate an increasing external field. This process can proceed until the total FRC toroidal current just equals the maximum possible synchronous electron current, at which time the RMF frequency would have to be increased to allow further temperature and confinement field increases. In the present experiments, with quartz first walls, our temperature appears to be limited by impurity radiation barriers, but we have still observed the above phenomena. Plans are underway to apply standard vacuum conditioning techniques on metal first walls to allow studies of non-radiation dominated power balance to be conducted.

1. Introduction

Rotating Magnetic Fields (RMF) have been used for many years in small, nearly spherical devices called rotamaks to produce compact toroids (CT), both with and without toroidal fields. In the most recent series of rotamak experiments the external confinement fields were supplied by simple solenoids and, if the RMF induced forces were high enough to form a CT, its flux simply increased until the plasma rested on external glass walls [1]. The RMF flux build-up and current drive technique has now been applied to standard prolate FRCs confined inside flux conserving coils in the Translation, Confinement, and Sustainment (TCS) device [2]. The FRCs can either be formed and sustained entirely by the applied RMF, or translated and expanded from a standard Field Reversed Theta Pinch (FRTP) and then sustained by the RMF.

A key feature of these experiments is the ability of the RMF to increase the FRC flux within an external flux conserver, so that as the FRC expands radially its external confinement field B_e will increase over the original bias field B_0 according to $B_e = B_0/(1-x_s^2)$. $x_s \equiv r_s/r_c$ is the ratio of separatrix radius to flux conserver radius. Both analytic [3] and numeric [4] models have been developed to explain this process. It has generally been assumed in this modeling that the cross-field resistivity η_{\perp} is a fixed value. The basic performance parameter is then the achievable plasma density n_e . $v_{ei} = n_e e^2 \eta_{\perp} / m_e$ must be much less than the electron cyclotron frequency $\omega_{ce} = eB_0/m_e$, where B_0 is the vacuum strength of the RMF. The plasma temperature is determined by power balance, although it is ultimately limited by the requirement that the maximum possible synchronous electron current, $I'_{syn} = 0.5 \langle n_e \rangle e \omega r_s^2$ be higher than the necessary field reversal current $I'_{rev} = 2B_0/\mu_0$, where ω is the RMF frequency.

2. Basic Theory

In a simple conductor the RMF would only penetrate a distance $\delta = (2\eta_{\perp}/\mu_0\omega)^{1/2}$. However, when the electrons are driven to a near synchronous frequency ω_e , such that the slip frequency $\varpi = \omega - \omega_e$ is small, the penetration distance will increase to $\delta^* = (2\eta_{\perp}/\mu_0\varpi)^{1/2}$. The slip frequency will adjust automatically to just carry the necessary reversal current such that $0.5n_m e \delta^* \omega_s \approx B_e/\mu_0$. n_m is the peak electron density and the factor of 0.5 arises because the RMF drives plasma inward so that the separatrix density is near zero, and the average density in the current carrying layer is $0.5n_m$. A positive E_{θ} will be generated as long as the total RMF induced torque exceeds the electron-ion frictional torque, and the FRC will expand radially (and contract axially depending on total energy and particle balance) against the flux conserver until the torques are in balance. This final steady-state condition is usually expressed as

$$\frac{\gamma}{\lambda} = \frac{0.007B_e(\text{G})}{n_m(10^{20}\text{ m}^{-3})\sqrt{D_{\perp}(\text{m}^2/\text{s})\omega(10^6\text{ s}^{-1})r_s^2(\text{m})}} = \frac{1}{\sqrt{2}}, \quad (1)$$

where $\gamma = \omega_{ce}/v_{ei}$, $\lambda = r_s/\delta$, and $D_{\perp} = \eta_{\perp}/\mu_0$. This relationship can be used to define an effective resistivity, or diffusivity, $D_{\perp} = (B_e/100)^2/\omega_s^2 n_m^2$ in the above units, based solely on the measured density. The analysis is essentially one-dimensional, does not take into account the ratios of RMF antenna length to FRC length, or end effects, but Eq. (1) is still a useful scaling relationship.

Due to the assumption of fixed resistivity, Eq. (1) says nothing about the plasma temperature or the achievable external field. In an elongated FRC the external field is given by radial pressure balance as $B_e(T) = 0.2[n_m(10^{20}\text{ m}^{-3})T_t(\text{keV})]^{1/2}$, with T_t being the sum of electron and ion temperatures. The penetration distance δ^* will then adjust, as specified above, to

$$\frac{\delta^*}{r_s} = \frac{0.02}{\omega(10^6\text{ s}^{-1})r_s^2(\text{m})}\sqrt{\frac{T_t(\text{keV})}{n_m(10^{20}\text{ m}^{-2})}}. \quad (2)$$

We usually use the parameter

$$\zeta = \frac{I'_{\text{rev}}}{I'_{\text{syn}}} = \frac{4B_e}{\mu_0\langle n_e \rangle e\omega r_s^2} = \frac{2}{\langle \beta \rangle} \frac{\delta^*}{r_s} \quad (3)$$

to represent whether there are sufficient electrons, if all were rotating synchronously with the RMF, to carry the reversal current. In our FRCs where radial expansion leads to $x_s \sim 0.85$ and $\langle \beta \rangle = 1 - 0.5x_s^2 \sim 0.65$, the RMF penetration would be $(\delta^*/r_s) \sim 0.3\zeta$, with a maximum value of 0.3 for $\zeta = 1$, a degree of penetration that corresponds to near optimal drive efficiency. This analysis is somewhat simplified, but is born out in overall features by numerical calculations. If the plasma temperature increased so high that δ^*/r_s exceeded about 0.3, the electrons would rotate faster than the RMF, and the RMF torque would become negative.

3. Experimental Measurements

A sketch of the TCS plasma chamber is shown on Fig. 1. The chamber consists of two 1.25-m long, 0.8-m diameter quartz tubes to allow RMF penetration, with vacuum access for diagnostics in between. Multi-turn main bias and end coils,

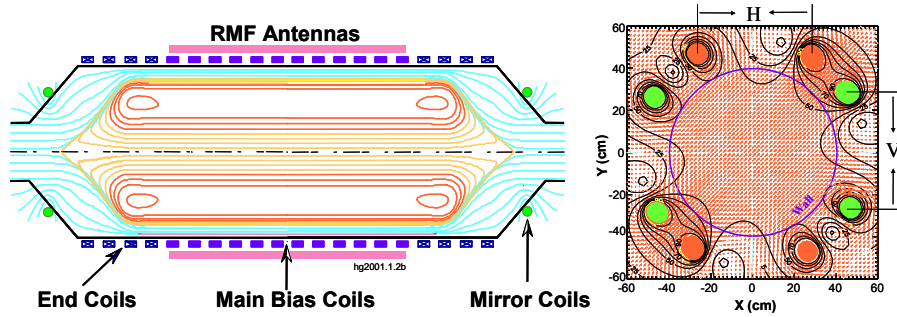


FIG. 1. TCS chamber showing end view of RMF antennas and resultant fields.

connected in parallel groups, supply the axial bias field B_0 . The effective flux conserver radius r_c is 0.47-m. The RMF antennas are arranged in two sets of Helmholtz-like pairs to promote field uniformity, and cover the central 1.6-m of the chamber. The 1.8 μH antennas are connected in parallel with capacitors to provide a resonant tank circuit. LANL-built RMF power supplies [5], operating at 12 kV can produce total antenna currents $I_{\text{ant}} = 10\sin(\omega t + \phi)$ kA at a typical 80 kHz frequency ($\omega = 0.5 \times 10^6 \text{ s}^{-1}$), resulting in an RMF with $B_0 = 64 \text{ G}$ when $\phi_H - \phi_V = 90^\circ$.

Typical measurements on an FRC formed from a preionized gas fill are shown on Fig. 2. An initial bias field of about 50 G is reversed by the application of the RMF, and the external flux is compressed, with B_e rising to 150 G. The internal field at $r = 0$ comes to about the same value, signifying a low separatrix pressure. The density is measured using a cross-tube CO_2 interferometer, and the total temperature is calculated from pressure balance. In all data presented T_t also includes the contribution of the B_0 component of the RMF to radial pressure. The absorbed RMF power was computed from the phase differences between antenna voltages and currents.

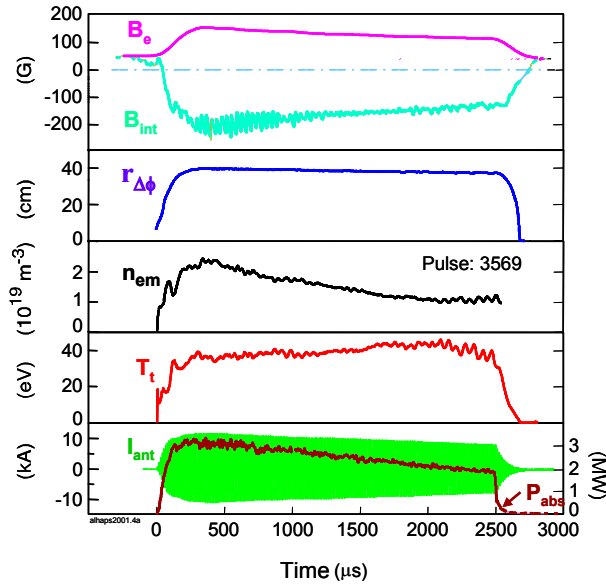


FIG. 2. RMF start-up operation at 80 kHz.

The axial confinement field (B_z) and the azimuthal component (B_x actually measured) of the RMF were measured with an internal array of (31) probes enclosed in a small diameter ceramic tube inserted radially at the center of TCS. At the relatively low temperatures of present operation the internal probe had no effect on overall performance. The profiles are shown on Fig. 3, along with an end-on sketch of the rotating field lines. For this case $\zeta \approx 0.2$ and the toroidal FRC current is only a fraction of its maximum possible value. The RMF only penetrates the outer layer of the FRC, but still reaches the field null. The profiles are in very good agreement with the analytic calculations of Ref. 3, despite the fact that the density is not uniform in the real FRC and the electrons only rotate near synchronously near the edge. Current

is maintained on the inner field lines due to an overall inward flow, which can be seen by applying a generalized Ohm's law, $E_\theta = \eta_\perp j_\theta + v_r B_z - \langle v_{ez} B_r \rangle$. On the outer flux surfaces the RMF drive term $\langle v_{ez} B_r \rangle$ must not only overcome the negative $\eta_\perp j_\theta$, but also must produce a negative $v_r B_z$. It is this negative v_r which counteracts resistivity on the inner (B_z negative) field lines.

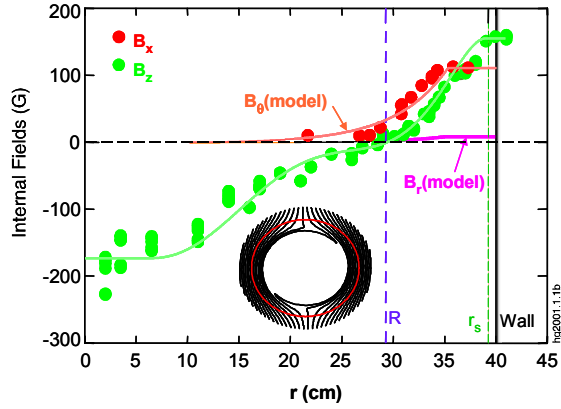


FIG. 3. Axial and rotating field profiles.

The total current drive process is extremely robust, with the density achieved related to the RMF drive and plasma resistivity (as long as sufficient particles are available), while the degree of penetration adjusts to that needed to produce the current necessary to reverse the external field, and hence relates to the plasma temperature. The absorbed power per unit length varies as

$$P'_{\text{abs}} \approx \frac{\eta_\perp (B_e / \mu_0)^2}{\delta^* / 2\pi r_s} \quad (4)$$

Since, at a given density, the penetration distance δ^* increases with B_e , the power absorption increases linearly with B_e . Detailed profile calculations and measurements show that the power absorption should be about half the value given by Eq. (4), but Eq. (4) as it stands appears to agree best with experimental measurements when values of η_\perp inferred from Eq. (1) are used. This can be partially accounted for by resistive losses of the axial shielding currents, but they are too small to fully account for the factor of two difference. Ultimate limits on absorbed power of about 5 MW are imposed by the intrinsic resistance of the LANL pulser.

The plasma resistivity inferred from Eq. (1) is shown in Fig. 4 for a series of runs at two RMF frequencies. (A point is also shown for the smaller $r_s = 0.2$ -m STX experiment running with $B_\omega = 20$ G and $\omega = 2.2 \times 10^6 \text{ s}^{-1}$.) The scaled resistivities appear to have an inverse density dependence. Higher densities could be achieved for the lower RMF frequencies, mainly due to the larger values of antenna current and B_ω that could be supplied at the lower antenna impedance. However, there was only a slight increase in density at the lower frequency for the same value of B_ω . This is reflected in the lower implied resistivities at the same density for the higher RMF frequency. The net result is that the achieved density appears to scale primarily only with some power of B_ω for reasons that are not presently understood.

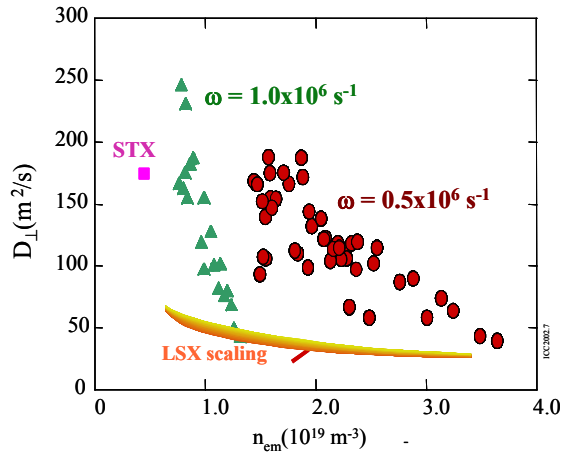


FIG. 4. Inferred plasma resistivities for RMF start-up experiments at two RMF frequencies.

For TCS operation with $\omega = 0.5 \times 10^6 \text{ s}^{-1}$, r_s is approximately 0.4 m, and Eq. (3) yields an upper limit of $T_{\text{max}}(\text{keV}) \approx 8B_e(\text{T})$. The resistivity scaling displayed in Fig. 4 results in a density scaling of $n_m(10^{20} \text{ m}^{-3}) = 0.62 \times 10^{-4} B_\omega^2(\text{G})$. Fig. 5 shows the plasma temperatures plotted against achieved external field, for RMF start-up cases with various values of B_ω . The lower limiting curve represents the value of density that could be achieved at the maximum $B_\omega = 70 \text{ G}$. The temperatures depended somewhat on initial fill densities, with higher

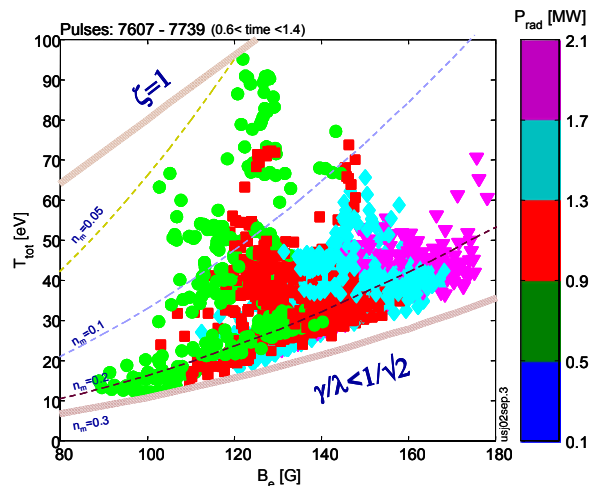


FIG.5. TCS RMF start-up results at $\omega = 0.5 \times 10^6 \text{ s}^{-1}$ for various B_ω and fill densities.

temperatures realized by restricting the initial fill density to the eventual final density, thus minimizing ionization and charge-exchange losses. The radiated power, indicated on Fig. 5, tended to scale as $n_e^2 T_t$, setting an upper limit on achievable temperature well below the $\zeta = 1$ limit. Higher temperatures could be achieved by further reducing the fill density, so that the densities specified by Eq. (1) could not be reached. These runs produced shorter FRCs that developed $n=2$ rotational instabilities and strongly interacted with the plasma tube wall and were not shown on Fig. 4. However, they do show the ability to approach the high penetration, $\zeta = 1$ limit.

4. Summary & Conclusions

The present work confirms the overall workings of RMF current drive in standard, prolate, flux-confined FRCs. The resistivity is high at the present low density conditions, perhaps due to very high values of ion drift velocity to ion thermal speed, or high values of B_ω/B_e , but the resistivity is decreasing rapidly as the density increases. Temperatures are presently limited by radiative losses, and modifications will be made to the TCS facility to provide metal first walls and wall conditioning commensurate with the now steady-state FRC operation.

References

- [1] EURIPEDES, P.E., JONES, I.R., DENG, C., "Rotamak discharges in a 0.5-m diameter spherical device", Nucl. Fusion **37**, (1997) 1505.
- [2] HOFFMAN, A.L. et. Al, "The TCS rotating magnetic field FRC current-drive experiment", Fusion Science & Technology **41**, (2002) 92.
- [3] HOFFMAN, A.L., "RMF current drive of FRCs subject to equilibrium constraints", Nucl. Fusion **40**, (2000) 1523.
- [4] MILROY, R.D., "An MHD model of RMF current drive in an FRC", Phys. Plasmas **7**, (2000) 4135.
- [5] TOBIN, S.J., et al, "The RMF amplifier system for current drive in the TCS experiment.", Rev. Sci. Instrum. **72**, (2001) 3528.